PRAMANA
— journal of
physics

Vol. 70, No. 1
January 2008
pp. 163–171

Anisotropic Hubbard model on a triangular lattice – spin dynamics in $HoMnO_3$

SAPTARSHI GHOSH and AVINASH SINGH*
Department of Physics, Indian Institute of Technology, Kanpur 208 016, India
*Corresponding author
E-mail: gsap@iitk.ac.in; avinas@iitk.ac.in

MS received 11 September 2006; revised 24 May 2007; accepted 28 August 2007

Abstract. The recent neutron scattering data for spin-wave dispersion in $HoMnO_3$ are well-described by an anisotropic Hubbard model on a triangular lattice with a planar (XY) spin anisotropy. Best fit indicates that magnetic excitations in $HoMnO_3$ correspond to the strong-coupling limit $U/t >\sim 15$, with planar exchange energy $J = 4t^2/U \simeq 2.5$ meV and planar anisotropy $\Delta U \simeq 0.35$ meV.

Keywords. Spin dynamics; neutron scattering; triangular lattice; multiferroics.

PACS Nos 75.50.Ee; 75.10.Lp; 75.30.Ds

There has been renewed interest in correlated electron systems on triangular lattices, as evidenced by recent studies of antiferromagnetism, superconductivity and metal–insulator transition in the organic systems κ-(BEDT-TTF)$_2$X [1,2], the discovery of superconductivity in $Na_xCoO_2 \cdot yH_2O$ [3], the observation of low-temperature insulating phases in some $\sqrt{3}$-adlayer structures such as K on Si[1 1 1], [4] and quasi-two-dimensional 120° spin ordering and spin-wave excitations in $RbFe(MoO_4)_2$ [5,6] and the multiferroic materials $YMnO_3$ and $HoMnO_3$ [7,8].

Recent neutron scattering studies of the multiferroic material $HoMnO_3$ have revealed a non-collinear 120° antiferromagnetic (AF) ordering below $T_N \approx 72$ K of the $S = 2$ Mn^{3+} spins arranged in offset layers of two-dimensional (2D) triangular lattice [7]. Measurements of the spin-wave dispersion were found to be well-described by a nearest-neighbour Heisenberg AF with exchange energy $J = 2.44$ meV and a planar anisotropy $D = 0.38$ meV at 20 K. No discernible dispersion was observed in the out-of-plane direction, indicating primarily 2D spin dynamics.

Recently spin-wave excitations in the 120° AF state of the Hubbard model on a triangular lattice were studied within the random phase approximation (RPA) in the full U range [9]. The spin-wave energy in the large U limit was shown to asymptotically approach the corresponding result for the quantum Heisenberg antiferromagnet (QHAF), thus providing a continuous interpolation between weak and strong coupling limits. However, competing interactions and frustration were

found to significantly modify the dispersion at finite U, resulting in vanishing spin stiffness at $U \approx 6$ and a magnetic instability at $U \approx 7$ corresponding to vanishing spin-wave energy at wave vector $\mathbf{q}_M = (\pi/3, \pi/\sqrt{3})$. The sharp fall-off of ω_M near $U \approx 7$ provides a sensitive indicator of finite-U effects in the AF state. Indeed, recent high-resolution neutron scattering studies of the spin-wave dispersion in the square-lattice $S = 1/2$ AF La_2CuO_4 have revealed noticeable spin-wave dispersion along the MBZ edge [10], associated with finite-U double-occupancy effects [11].

In this report we extend the spin-wave analysis to include planar spin anisotropy, and show that the neutron scattering data for $HoMnO_3$ are also well-described by a Hubbard model on a triangular lattice, thus providing a microscopic description of the most essential features of spin dynamics in the 120° AF state of $HoMnO_3$, including the spin-wave dispersion and energy scale. We examine the behaviour of spin-wave anisotropy gap with spin anisotropy and also suggest a sensitive measure of finite-U, double occupancy effects.

However, the Mn spin planar anisotropy is treated here only at a phenomenological level, equivalent to the effective anisotropy DS_{iz}^2 included in recent investigations using spin models [7,8]. Microscopically, magnetocrystalline anisotropy originates from two important mechanisms resulting in the single-ion anisotropy ($\mathbf{S}_i \cdot \mathbf{D} \cdot \mathbf{S}_i$) and the two-ion anisotropic exchange ($\mathbf{S}_i \cdot \mathbf{J}_{ij} \cdot \mathbf{S}_j$) in the magnetic Hamiltonian.

The mechanism of single-ion anisotropy generally involves (i) an asymmetric crystal field, (ii) a non-zero orbital angular momentum for the highest occupied electronic state so that the orbital senses the crystal field symmetry, and (iii) a non-zero spin-orbit interaction for the spin to couple to the crystal field [12]. The single-ion anisotropy results from a second-order correction to the ground-state energy where the spin-orbit coupling $\mathbf{L} \cdot \mathbf{S}$ is treated as a perturbation and the crystal-field levels form the unperturbed states, yielding a spin-space angular dependence in the ground-state energy [13].

In a recent study of single-ion anisotropy and crystal-field effects in the layered rare-earth cuprates R_2CuO_4 (R = Nd, Pr, Sm), the magnetic behaviour (including spin-reorientation transitions) has been attributed to the coupling of Cu with the rare-earth magnetic subsystem [14]. Treating the Cu–R interaction within the mean-field approximation, the authors consider the Hamiltonian

$$\mathcal{H} = \mathcal{H}_{\mathrm{CEF}} - \mathbf{J} \cdot \mathbf{h} \tag{1}$$

for the rare-earth ion in the presence of an exchange field $\mathbf{h}$ due to Cu spins. Here $\mathcal{H}_{\mathrm{CEF}}$ is the crystal electric field (CEF) potential, and the authors have restricted their treatment to states in the lowest $\mathbf{J}$ multiplet. Treating the exchange interaction $-\mathbf{J} \cdot \mathbf{h}$ as a perturbation, the ground-state energy was shown to exhibit anisotropic dependence on the exchange field, resulting in preferential ordering of rare-earth moments along specific lattice directions.

The anisotropy of Mn spins in $HoMnO_3$, its observed temperature dependence, and the reorientation transitions have been suggested to originate from a similar anisotropic exchange coupling with the rare-earth holmium [7], resulting in magnetic behaviour as seen in layered rare-earth cuprates, where frustrated interlayer coupling allows for weaker, higher-order interactions to control the magnetic structure.

In contrast, with regard to the two-ion anisotropic exchange mechanism, the Dzyaloshinski-Moriya (DM) antisymmetric exchange interaction $\mathbf{D} \cdot (\mathbf{S}_i \times \mathbf{S}_j)$ was

shown to originate from spin-orbit coupling in combination with a crystal potential of sufficiently low symmetry [15,16]. The spin-orbit term of the form $i[\mathbf{f}\cdot\boldsymbol{\sigma}]_{\sigma\sigma'}a^\dagger_{i\sigma}a_{j\sigma'}$, where $\mathbf{f}\sim\boldsymbol{\nabla}V(r)\times\mathbf{p}$, represents spin-dependent hopping, and results in the above DM interaction from the same strong-coupling expansion which yields the isotropic exchange interaction $\mathbf{S}_i\cdot\mathbf{S}_j$ from the usual real spin-independent hopping.

Especially relevant for non-collinear ordering, the DM interaction has been suggested as being responsible for the clamping of ferroelectric and antiferromagnetic order parameters in $YMnO_3$ [17]. In La_2CuO_4, the Dzyaloshinski-Moriya (DM) antisymmetric exchange term is allowed by the orthorhombic distortion, which is also responsible for the net interlayer exchange interaction, and the resulting anisotropy gap controls the low-temperature magnetic dynamics [18]. The role of spin-orbit coupling and DM interaction has also been highlighted in the context of long-period spiral spin density waves in the itinerant helimagnet MnSi, studied within a single-band Hubbard model with spin-orbit coupling [19], and within the Landau–Ginzburg formalism [20,21].

Hund's rule coupling responsible for the $S=2$ spin state of Mn^{3+} ions and crystal-field splitting have also not been realistically incorporated here. However, these realistic details do not qualitatively affect the spin-rotation symmetry and spin dynamics, as discussed below. Hund's rule coupling in the generalized Hubbard model considered here is maximal as inter-orbital Coulomb interaction for parallel spins is dropped completely. Including an inter-orbital density–density interaction V_0 and an intra-atomic exchange interaction F_0 favouring parallel-spin alignment (Hund's rule coupling), the more realistic orbital Hubbard model [22,23]

$$\begin{aligned} H = & -t\sum_{i,\delta,\gamma,\sigma} a^\dagger_{i\gamma\sigma}a_{i+\delta,\gamma\sigma} + U\sum_{i\gamma} n_{i\gamma\uparrow}n_{i\gamma\downarrow} \\ & + \sum_{i,\gamma<\gamma',\sigma,\sigma'} (V_0-\delta_{\sigma\sigma'}F_0)n_{i\gamma\sigma}n_{i\gamma'\sigma'} \\ & + F_0\sum_{i,\gamma<\gamma',\sigma\neq\sigma'} a^\dagger_{i\gamma\sigma}a_{i\gamma'\sigma}a^\dagger_{i\gamma'\sigma'}a_{i\gamma\sigma'} \end{aligned} \tag{2}$$

remains spin-rotationally invariant under a global rotation of the fermion spin $\mathbf{S}_{i\gamma}=\Psi^\dagger_{i\gamma}(\boldsymbol{\sigma}/2)\Psi_{i\gamma}$ (where $\Psi^\dagger_{i\gamma}\equiv(a^\dagger_{i\gamma\uparrow}\ a^\dagger_{i\gamma\downarrow})$ is the fermion field operator), even if orbitals γ are identified with the Mn orbitals (t_{2g},e_g) resulting from crystal-field splitting of the atomic 3d orbitals. As the intra-atomic exchange interaction F_0 is much larger than the spin excitation energy scale ($\sim\frac{t^2}{U+F_0}$, within a strong-coupling expansion), all fermion spins on a site are effectively coupled, yielding a composite quantum spin S and a corresponding multiplication by factor $2S$ to obtain the effective spin-wave energy scale. Therefore, orbital multiplicity does not change the Goldstone-mode structure, and the spin-dynamics energy scale in the orbital Hubbard model is essentially determined by t and $U_{\rm eff}=U+F_0$.

As the simplest extension to phenomenologically include spin-space anisotropy, while retaining only the relevant energy scales t and $U_{\rm eff}$, we consider the generalized $\mathcal{N}$-orbital Hubbard model [24]

$$H = -t \sum_{i,\delta,\gamma,\sigma} a^\dagger_{i\gamma\sigma} a_{i+\delta,\gamma,\sigma} + \frac{U_1}{\mathcal{N}} \sum_{i,\gamma,\gamma'} a^\dagger_{i\gamma\uparrow} a_{i\gamma\uparrow} a^\dagger_{i\gamma'\downarrow} a_{i\gamma'\downarrow} + \frac{U_2}{\mathcal{N}} \sum_{i,\gamma,\gamma'} a^\dagger_{i\gamma\uparrow} a_{i\gamma'\uparrow} a^\dagger_{i\gamma'\downarrow} a_{i\gamma\downarrow} \tag{3}$$

on a triangular lattice with nearest-neighbour (NN) hopping between sites i and $i+\delta$. Here γ, γ' refer to the (fictitious) degenerate $\mathcal{N}$ orbitals per site. The factor $\frac{1}{\mathcal{N}}$ is included to render the energy density finite in the $\mathcal{N} \to \infty$ limit. The two correlation terms involve density–density and exchange interactions with respect to the orbital indices. The Hartree–Fock (HF) approximation and random phase approximation (RPA) are of $O(1)$ whereas quantum fluctuation effects appear at higher order within the inverse-degeneracy expansion and thus $1/\mathcal{N}$, in analogy with $1/S$ for quantum spin systems, plays the role of $\hbar$.

The key feature of spin-rotation symmetry of the generalized Hubbard model is highlighted by writing the two interaction terms as

$$H_{\rm int} - \frac{U_2}{\mathcal{N}} \sum_i \mathbf{S}_i \cdot \mathbf{S}_i + \frac{U_2 - U_1}{\mathcal{N}} \sum_i S^2_{iz} \tag{4}$$

in terms of the total spin operator

$$\mathbf{S}_i = \sum_\gamma \psi^\dagger_{i\gamma} \frac{\boldsymbol{\sigma}}{2} \psi_{i\gamma} \equiv \sum_\gamma \frac{\boldsymbol{\sigma}_{i\gamma}}{2}, \tag{5}$$

where $\psi^\dagger_{i\gamma} \equiv (a^\dagger_{i\gamma\uparrow}\ a^\dagger_{i\gamma\downarrow})$. An Ising (uniaxial) anisotropy is obtained for $U_1 > U_2$, a planar (XY) anisotropy for $U_2 > U_1$, and full spin-rotation symmetry for $U_1 = U_2$.

As appropriate for $HoMnO_3$, we consider the case $U_2 > U_1$ corresponding to preferential ordering of spins in the x–y plane in spin space and an anisotropy gap for out-of-plane excitations [7]. Magnetic excitations were analyzed in terms of a Heisenberg model with a similar anisotropy term in ref. [7]. At the HF level, the interaction term for orbital γ then reduces to

$$H^\gamma_{\rm int} - \sum_i \boldsymbol{\sigma}_{i\gamma} \cdot \boldsymbol{\Delta}_i, \tag{6}$$

where the self-consistently determined mean field $\boldsymbol{\Delta}_i = U_2 \langle \mathbf{S}_{i\gamma'} \rangle_{\rm HF}$ lies in the x–y plane in spin space. The HF sublattice magnetization depends only on U_2 and is determined from the self-consistency condition $\langle \mathbf{S}_\alpha \rangle_{\rm HF} \sum_{\mathbf{k},l} \langle \mathbf{k}, l | (\boldsymbol{\sigma}/2) | \mathbf{k}, l \rangle_\alpha$ in terms of the HF states $|\mathbf{k}, l\rangle$ on sublattice α, exactly as for the isotropic case [9]. In the strong coupling limit, the sublattice magnetization $\langle \mathbf{S}_\alpha \rangle \approx 1/2$ at the HF level, and is reduced by about 50% (in the isotropic case) due to quantum fluctuations, as found in different calculations cited in ref. [9].

We consider the 120° ordered AF state on the triangular lattice, and examine transverse spin fluctuations about the broken-symmetry state. At the RPA level, the magnon propagator reduces to a sum of all bubble diagrams where the interaction vertices involving S^2_{ix} and S^2_{iy} appear with interaction U_2, whereas those involving S^2_{iz} with interaction U_1. Introducing a planar spin rotation, so that spins

are oriented along the x' direction for all three sublattices, we obtain for the transverse spin-fluctuation propagator

$$[\chi(\mathbf{q},\omega)]^{\mu\nu}_{\alpha\beta} = \frac{[\chi^0(\mathbf{q},\omega)]}{\mathbf{1} - 2[U][\chi^0(\mathbf{q},\omega)]} \tag{7}$$

in the $2 \otimes 3$ spin-sublattice basis of the two transverse spin directions $\mu, \nu = y', z'$ and the three sublattices $\alpha, \beta = A, B, C$. The sublattice-diagonal interaction matrix

$$[U] = \begin{bmatrix} U_2\mathbf{1} & \mathbf{0} \\ \mathbf{0} & U_1\mathbf{1} \end{bmatrix} \tag{8}$$

in the y', z' basis, and the bare particle–hole propagator

$$[\chi^0(\mathbf{q},\omega)]^{\mu\nu}_{\alpha\beta} = \frac{1}{4}\sum_{\mathbf{k},l,m}\left[\frac{\langle\sigma_\mu\rangle^{-+}_{\alpha}\langle\sigma_\nu\rangle^{-+*}_{\beta}}{E^{+}_{\mathbf{k}-\mathbf{q},m} - E^{-}_{\mathbf{k},l} + \omega} + \frac{\langle\sigma_\mu\rangle^{+-}_{\alpha}\langle\sigma_\nu\rangle^{+-*}_{\beta}}{E^{+}_{\mathbf{k},m} - E^{-}_{\mathbf{k}-\mathbf{q},l} - \omega}\right] \tag{9}$$

involves integrating out the fermions in the broken-symmetry state. In the particle–hole matrix elements

$$\langle\sigma_\mu\rangle^{-+}_{\alpha} \equiv \langle\mathbf{k}-\mathbf{q}, m|\sigma_\mu|\mathbf{k}, l\rangle_\alpha \tag{10}$$

of the rotated spins, the spin orientation angles ϕ_α in the fermion states $|\mathbf{k}, l\rangle$ are transformed out. The numerical evaluation of $[\chi^0(\mathbf{q},\omega)]$ in terms of the HF-level AF-state energies and amplitudes is exactly as for the isotropic case studied earlier [9].

The spin-wave energies $\omega_\mathbf{q}$ are then obtained from the poles $1 - \lambda_\mathbf{q}(\omega_\mathbf{q}) = 0$ of eq. (7) in terms of the eigenvalues $\lambda_\mathbf{q}(\omega)$ of the matrix $2[U][\chi^0(\mathbf{q},\omega)]$. As $\omega_\mathbf{q}$ corresponds to spin-1/2, it is scaled by the factor $2S$ for arbitrary spin S [25]. As expected for planar anisotropy, there is only one Goldstone mode corresponding to planar rotation of spins, and the two out-of-plane modes become massive with an anisotropy gap $\omega_{\rm gap}$.

Spin-wave dispersion $\omega_\mathbf{q}$ for the three modes is shown in figure 1 along two symmetry directions in the magnetic Brillouin zone (MBZ), along with the neutron scattering data for $HoMnO_3$ at 20 K from ref. [7]. The anisotropic Hubbard model provides a remarkably good description of the spin dynamics. We find that best fits with the magnetic excitations in $HoMnO_3$ are only obtained in the strong-coupling limit $U/t > \sim 15$, with a planar exchange energy $J = 4t^2/U \simeq 2.5$ meV and anisotropy $U_2 - U_1 \equiv \Delta U \simeq 0.35$ meV, the individual values of t and U not being resolvable within experimental resolution. To estimate the order of magnitude of the ratio U/t, if we nominally take $U = 1$ eV, we obtain $t = 25$ meV and $U/t = 40$. Spin-wave dispersion calculated in the intermediate coupling regime cannot be fitted with the neutron scattering data, indicating no evidence of finite-U double occupancy effects, as discussed below.

For the square-lattice $S = 1/2$ AF La_2CuO_4, finite-U, double-occupancy effects associated with higher-order (t^4/U^3) spin couplings are manifested in noticeable

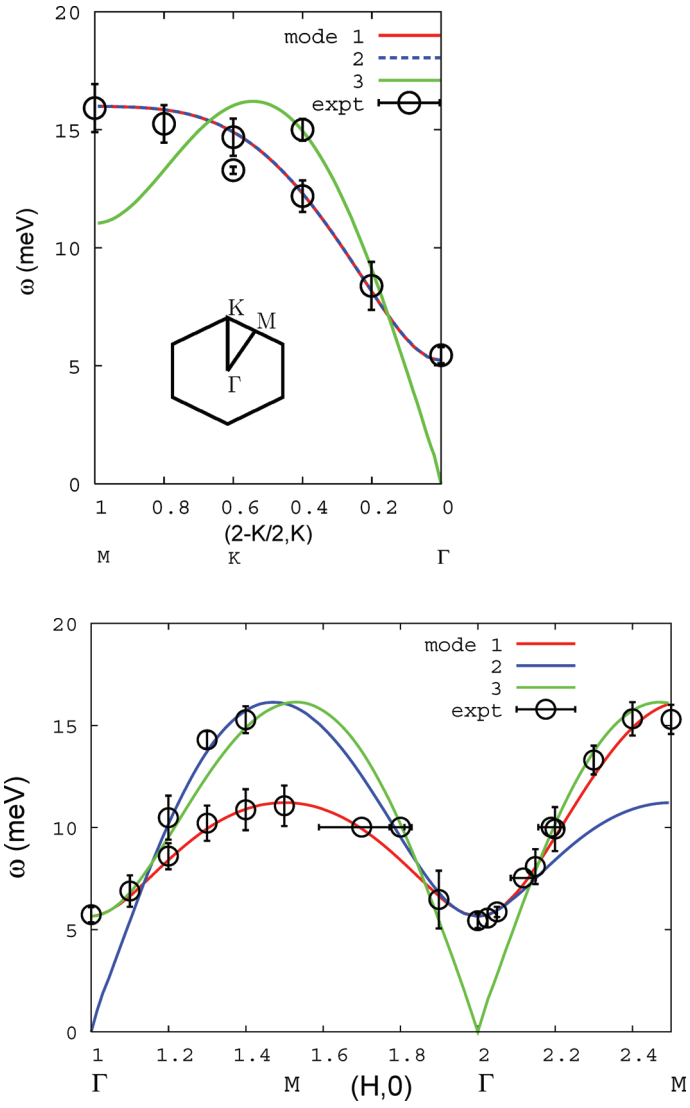

Figure 1. Spin-wave dispersion for the three modes calculated from eq. (7) with $J = 4t^2/U \approx 2.5$ meV and $\Delta U \approx 0.35$ meV, along with neutron scattering data points for $HoMnO_3$ at 20 K from ref. [7].

spin-wave dispersion along the MBZ boundary [10,11]. Similarly, for the isotropic triangular lattice AF, the ratio $\omega_1/\omega_{2,3}$ of the non-degenerate and degenerate spin-wave energies at wave vector $\mathbf{q}_M = (\pi/3, \pi/\sqrt{3})$ is a sensitive measure of the U/t ratio [9], which asymptotically approaches $2/\sqrt{10} = 0.632$ in the strong-coupling ($U/t \to \infty$) limit, decreases monotonically with U/t, and eventually vanishes at $U/t \approx 7$ [9]. Variation of $\omega_1/\omega_{2,3}$ with U/t is shown in figure 2 for different values of anisotropy $\Delta U/t$. Neutron scattering data for $HoMnO_3$ show that $\omega_1/\omega_{2,3} \approx$

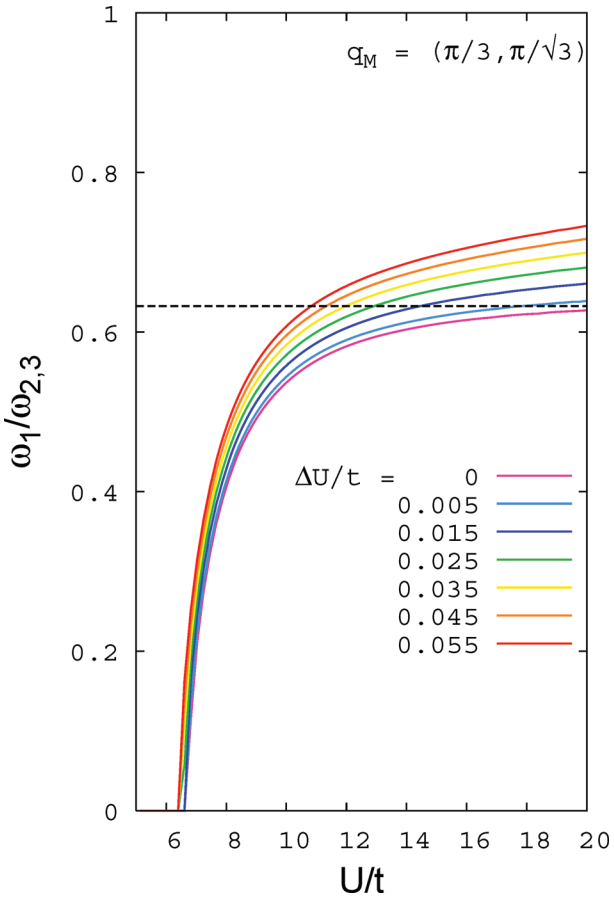

Figure 2. The ratio $\omega_1/\omega_{2,3}$ at wave vector $\mathbf{q}_M$ provides a sensitive indicator of finite-U, double-occupancy effects, shown for different values of spin anisotropy ΔU.

11 meV/16 meV ≈ 0.7, which yields a lower bound ($\sim$15) on the ratio U/t from figure 2.

The spin-wave anisotropy gap $\omega_{\rm gap}/t$, corresponding to out-of-plane fluctuations with $q = 0$, varies as $(\Delta U/U)^{1/2}$ with spin anisotropy (figure 3), which translates to $\omega_{\rm gap} \propto \sqrt{J\Delta U}$, the geometric mean of the two energy scales.

In conclusion, the anisotropic Hubbard model provides a simple extension to phenomenologically include spin-space anisotropy and study spin excitations in the full range from weak to strong coupling. Comparison of spin-wave dispersion with RPA calculations allows for a quantitative determination of the effective anisotropy, in addition to highlighting any finite-U, double occupancy effects as seen in La_2CuO_4. The recent neutron scattering data for spin-wave dispersion in $HoMnO_3$ are found to be well-described by an anisotropic Hubbard model on a triangular lattice with a planar (XY) spin anisotropy. We find that the twin constraints $\omega_{\rm gap}/\omega_{1,2} \approx 1/3$ and

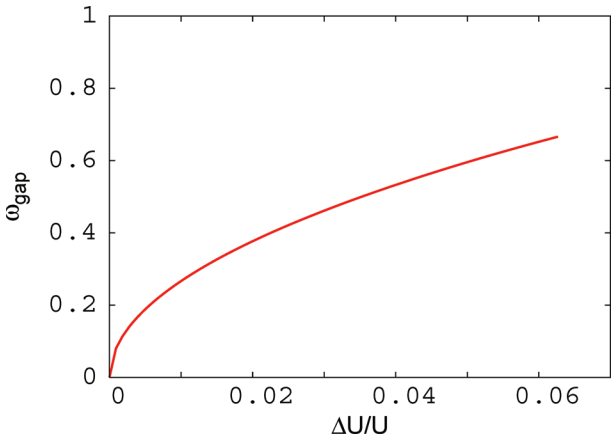

Figure 3. Spin-wave anisotropy gap corresponding to out-of-plane fluctuations shows a $\sim(\Delta U/U)^{1/2}$ behaviour with spin anisotropy. Here $U/t = 16$.

$\omega_1/\omega_{2,3} \approx 2/3$ in the neutron scattering data cannot be satisfied in the intermediate coupling regime, and best fit indicates that magnetic excitations in $HoMnO_3$ correspond to the strong-coupling limit $U/t > \sim 15$, with $J \simeq 2.5$ meV and $\Delta U \simeq 0.35$ meV. The ratio $\omega_1/\omega_{2,3}$ of the non-degenerate and degenerate spin-wave energies at wave vector $\mathbf{q}_M = (\pi/3, \pi/\sqrt{3})$ is suggested as a sensitive measure of finite-U, double occupancy effects in a triangular-lattice antiferromagnet. Finally, in view of the formal resemblance with the orbital Hubbard model (2), our RPA calculation provides a step forward towards investigating magnetic excitations using realistic models including Hund's rule coupling, crystal-field splitting etc.

References

[1] K Kanoda, *Physica* **C282–287**, 299 (1997); *Hyperfine Interact.* **104**, 235 (1997)
[2] R H McKenzie, *Science* **278**, 820 (1997)
[3] K Takada *et al*, *Nature (London)* **422**, 53 (2003)
[4] H H Weitering, X Shi, P D Johnson, J Chen, N J Dinardo and S Kempa, *Phys. Rev. Lett.* **78**, 1331 (1997)
[5] T Inami, Y Ajiro and T Goto, *J. Phys. Soc. Jpn.* **65**, 2374 (1996)
[6] L E Svistov, A I Smirnov, L A Prozorova, O A Petrenko, L N Demianets and A Ya Shapiro, *Phys. Rev.* **B67**, 094434 (2003)
[7] O P Vajk, M Kenzelmann, J W Lynn, S B Kim and S-W Cheong, *Phys. Rev. Lett.* **94**, 087601 (2005)
[8] T J Sato, S-H Lee, T Katsufuji, M Masaki, S Park, J R D Copley and H Takagi, *Phys. Rev.* **B68**, 014432 (2003)
[9] A Singh, *Phys. Rev.* **B71**, 214406 (2005)
[10] R Coldea, S M Hayden, G Aeppli, T G Perring, C D Frost, T E Mason, S-W Cheong and Z Fisk, *Phys. Rev. Lett.* **86**, 5377 (2001)
[11] A Singh and P Goswami, *Phys. Rev.* **B66**, 92402 (2002)
[12] R C O'Handley, *Modern magnetic materials: Principles and applications* (Wiley, New York, 2000) p. 198

[13] T Murao, in *The structure and properties of matter* edited by T Matsubara (Springer, Berlin, 1982) pp. 293–296
[14] R Sachidanandam, T Yildirim, A B Harris, A Aharony and O E Wohlman, *Phys. Rev.* **B56**, 260 (1997)
[15] I Dzyaloshinsky, *J. Phys. Chem. Colloids* **4**, 241 (1958)
[16] T Moriya, *Phys. Rev.* **120**, 91 (1960)
[17] E Hanamura, K Hagita and Y Tanabe, *J. Phys.: Condens. Matter* **15**, L103 (2003)
[18] A Singh and Z Tešanović, *Phys. Rev.* **B43**, 11445 (1990)
[19] T A Kaplan, *Z. Physik* **B49**, 313 (1983)
[20] B Binz, A Vishwanath and V Aji, *Phys. Rev. Lett.* **96**, 207202 (2006)
[21] B Binz and A Vishwanath, *Phys. Rev.* **B74**, 214408 (2006)
[22] L M Roth, *Phys. Rev.* **149**, 306 (1966)
[23] K Held and D Vollhardt, *Euro. Phys. J.* **B5**, 473 (1998)
[24] A Singh, *Phys. Rev.* **B43**, 3617 (1991)
[25] A Singh and P Sen, *Phys. Rev.* **B57**, 10598 (1998)